Upper limits for the photoproduction cross section for the Φ^{−−}(1860) pentaquark state off the deuteron

H. Egiyan *et al.* (CLAS Collaboration)

Upper limits for the photoproduction cross section for the $\Phi^{--}(1860)$ pentaquark state off the deuteron

H. Egiyan,[1,2] J. Langheinrich,[3] R.W. Gothe,[3] L. Graham,[3] M. Holtrop,[1] H. Lu,[10,3] P. Mattione,[10,4] G. Mutchler,[4,*]
K. Park,[2,3] E.S. Smith,[2] S. Stepanyan,[2] Z.W. Zhao,[40,3] K.P. Adhikari,[33] M. Aghasyan,[23] M. Anghinolfi,[24]
H. Baghdasaryan,[40,33] J. Ball,[12] N.A. Baltzell,[3,†] M. Battaglieri,[24] I. Bedlinskiy,[27] R. P. Bennett,[33] A.S. Biselli,[16,10]
C. Bookwalter,[18] D. Branford,[15] W.J. Briscoe,[20] W.K. Brooks,[38,2] V.D. Burkert,[2] D.S. Carman,[2] A. Celentano,[24]
S. Chandavar,[32] M. Contalbrigo,[22] A. D'Angelo,[25,36] A. Daniel,[32] N. Dashyan,[42] R. De Vita,[24] E. De Sanctis,[23]
A. Deur,[2] B. Dey,[10] R. Dickson,[10] C. Djalali,[3] D. Doughty,[13,2] R. Dupre,[5] A. El Alaoui,[5] L. El Fassi,[5] P. Eugenio,[18]
G. Fedotov,[3] S. Fegan,[39] A. Fradi,[26] M.Y. Gabrielyan,[17] N. Gevorgyan,[42] G.P. Gilfoyle,[35] K.L. Giovanetti,[28]
F.X. Girod,[2] J.T. Goetz,[7] W. Gohn,[14] E. Golovatch,[37] K.A. Griffioen,[41] M. Guidal,[26] N. Guler,[33,‡] L. Guo,[17,2]
V. Gyurjyan,[2] K. Hafidi,[5] H. Hakobyan,[38,42] C. Hanretty,[40] D. Heddle,[13,2] K. Hicks,[32] Y. Ilieva,[3,20] D.G. Ireland,[39]
B.S. Ishkhanov,[37] H.S. Jo,[26] K. Joo,[14] P. Khetarpal,[17] A. Kim,[29] W. Kim,[29] A. Klein,[33] F.J. Klein,[11]
V. Kubarovsky,[2,34] S.V. Kuleshov,[38,27] K. Livingston,[39] I.J.D. MacGregor,[39] Y. Mao,[3] M. Mayer,[33] B. McKinnon,[39]
V. Mokeev,[2,37,§] E. Munevar,[20] P. Nadel-Turonski,[2] A. Ni,[29] G. Niculescu,[28] A.I. Ostrovidov,[18] M. Paolone,[3]
L. Pappalardo,[22] R. Paremuzyan,[42] S. Park,[18] E. Pasyuk,[2,6] S. Anefalos Pereira,[23] E. Phelps,[3] O. Pogorelko,[27]
S. Pozdniakov,[27] J.W. Price,[8] S. Procureur,[12] D. Protopopescu,[39] B.A. Raue,[17,2] G. Ricco,[19,¶] D. Rimal,[17]
M. Ripani,[24] B.G. Ritchie,[6] G. Rosner,[39] P. Rossi,[23] F. Sabatié,[12] M.S. Saini,[18] C. Salgado,[31] D. Schott,[17]
R.A. Schumacher,[10] E. Seder,[14] H. Seraydaryan,[33] Y.G. Sharabian,[2] G.D. Smith,[39] D.I. Sober,[11] S.S. Stepanyan,[29]
S. Strauch,[3,20] M. Taiuti,[19,¶] W. Tang,[32] C.E. Taylor,[21] D.J. Tedeschi,[3] M. Ungaro,[14,34] E. Voutier,[30]
D.P. Watts,[15] L.B. Weinstein,[33] D.P. Weygand,[2] M.H. Wood,[9,3] N. Zachariou,[20] L. Zana,[1] and B. Zhao[41]

(The CLAS Collaboration)

[1]*University of New Hampshire, Durham, New Hampshire 03824-3568*
[2]*Thomas Jefferson National Accelerator Facility, Newport News, Virginia 23606*
[3]*University of South Carolina, Columbia, South Carolina 29208*
[4]*Rice University, Houston, Texas 77005-1892*
[5]*Argonne National Laboratory, Argonne, Illinois 60441*
[6]*Arizona State University, Tempe, Arizona 85287-1504*
[7]*University of California at Los Angeles, Los Angeles, California 90095-1547*
[8]*California State University, Dominguez Hills, Carson, CA 90747*
[9]*Canisius College, Buffalo, NY*
[10]*Carnegie Mellon University, Pittsburgh, Pennsylvania 15213*
[11]*Catholic University of America, Washington, D.C. 20064*
[12]*CEA, Centre de Saclay, Irfu/Service de Physique Nucléaire, 91191 Gif-sur-Yvette, France*
[13]*Christopher Newport University, Newport News, Virginia 23606*
[14]*University of Connecticut, Storrs, Connecticut 06269*
[15]*Edinburgh University, Edinburgh EH9 3JZ, United Kingdom*
[16]*Fairfield University, Fairfield CT 06824*
[17]*Florida International University, Miami, Florida 33199*
[18]*Florida State University, Tallahassee, Florida 32306*
[19]*Università di Genova, 16146 Genova, Italy*
[20]*The George Washington University, Washington, DC 20052*
[21]*Idaho State University, Pocatello, Idaho 83209*
[22]*INFN, Sezione di Ferrara, 44100 Ferrara, Italy*
[23]*INFN, Laboratori Nazionali di Frascati, 00044 Frascati, Italy*
[24]*INFN, Sezione di Genova, 16146 Genova, Italy*
[25]*INFN, Sezione di Roma Tor Vergata, 00133 Rome, Italy*
[26]*Institut de Physique Nucléaire ORSAY, Orsay, France*
[27]*Institute of Theoretical and Experimental Physics, Moscow, 117259, Russia*
[28]*James Madison University, Harrisonburg, Virginia 22807*
[29]*Kyungpook National University, Daegu 702-701, Republic of Korea*
[30]*LPSC, Universite Joseph Fourier, CNRS/IN2P3, INPG, Grenoble, France*
[31]*Norfolk State University, Norfolk, Virginia 23504*
[32]*Ohio University, Athens, Ohio 45701*
[33]*Old Dominion University, Norfolk, Virginia 23529*
[34]*Rensselaer Polytechnic Institute, Troy, New York 12180-3590*
[35]*University of Richmond, Richmond, Virginia 23173*
[36]*Universita' di Roma Tor Vergata, 00133 Rome Italy*
[37]*Skobeltsyn Nuclear Physics Institute, Skobeltsyn Nuclear Physics Institute, 119899 Moscow, Russia*

^{38}*Universidad Técnica Federico Santa María, Casilla 110-V Valparaíso, Chile*
^{39}*University of Glasgow, Glasgow G12 8QQ, United Kingdom*
^{40}*University of Virginia, Charlottesville, Virginia 22901*
^{41}*College of William and Mary, Williamsburg, Virginia 23187-8795*
^{42}*Yerevan Physics Institute, 375036 Yerevan, Armenia*
(Dated: December 5, 2011)

We searched for the $\Phi^{--}(1860)$ pentaquark in the photoproduction process off the deuteron in the $\Xi^-\pi^-$ decay channel using CLAS. The invariant mass spectrum of the $\Xi^-\pi^-$ system does not indicate any statistically significant enhancement near the reported mass $M = 1.860$ GeV. The statistical analysis of the sideband-subtracted mass spectrum yields a 90% confidence level upper limit of 0.7 nb for the photoproduction cross section of $\Phi^{--}(1860)$ with a consecutive decay into $\Xi^-\pi^-$ in the photon energy range 4.5 GeV $< E_\gamma <$ 5.5 GeV.

PACS numbers: 14.20.Jn, 14.20.Pt, 13.60.Rj, 12.39.-x

I. INTRODUCTION

Narrow bound states of four quarks and one anti-quark have been the focus of intense searches since the report by the LEPS collaboration of a positively charged baryon called the Θ^+, with $S = +1$ and a mass of 1.54 GeV [1] . This "exotic" combination of quantum numbers cannot be accommodated within the simple quark model, which assumes that all baryons are built out of three quarks. Exotic states of this kind have been predicted within the Chiral Soliton Model [2] as part of a spin 1/2 anti-decuplet of baryons. The anti-decuplet of "pentaquarks" contains three explicitly exotic states, whose quantum numbers require a minimal quark content of four quarks and one anti-quark. Reference [3] describes the experimental situation for $\Theta^+(1540)$ searches, and a concise summary of the current state of pentaquarks can also be found in the Particle Data Group (PDG) review [4].

The two other exotic states of the anti-decuplet have charge $Q = -2$ (quark content of $ddss\overline{u}$) and $Q = +1$ (quark content of $uuss\overline{d}$). Their strangeness is $S = -2$, but they have isospin 3/2, in contrast to normal cascade states with isospin 1/2. The Particle Data Group [4] has assigned the name of $\Phi(1860)$ to the four states in the strangeness $S = -2$ sector of the anti-decuplet. The NA49 collaboration has reported evidence for the strangeness $S = -2$ pentaquark Φ^{--} and the Φ^0 at a mass of 1.862 GeV [5]. This measurement was conducted in $p+p$ collisions at a center-of-mass energy $\sqrt{s} = 17.2$ GeV, and the states were reconstructed from their decays into the ground state cascades, $\Phi^{--} \rightarrow \Xi^-\pi^-$ and $\Phi^0 \rightarrow \Xi^-\pi^+$. We also note that many experiments [6–20], some of which represent a much larger statistical

Source	Mass (GeV)
Chiral-Soliton Model [2, 21]	2.07 [1.86]
Chiral-Soliton Model [24]	1.79-1.97
Diquark Model [22, 25]	1.75
Diquark-Triquark Model [23, 26]	1.783
Experiment NA49 [5]	1.862 ± 0.002

TABLE I: Selected representative model expectations for the mass of the cascade pentaquark. Note that the first entry gives the initial prediction of the Chiral-Soliton model of 2.07 GeV, followed in square brackets with the adjusted model to the experimental value of NA49.

sample, have not been able to confirm the NA49 observation [5].

Guidance for where and how to search for cascade pentaquarks is very sparse. The mass scale for the Θ^+ can be estimated to be about the mass of the nucleon (0.94 GeV) plus the mass of the kaon (0.5 GeV). The mass of the cascade pentaquark contains an additional strange quark, which naively would lead to 1.89 GeV, assuming that the strange and anti-strange quarks have the same mass of about 0.45 GeV. The quark model predictions vary depending on the amount of mixing between the anti-decuplet and octet members, as well as the estimated size of the color-spin hyperfine interaction between quarks. We also note that some of the models [21–23] have used the experimental reports of either the $\Theta^+(1540)$ or $\Phi(1860)$, or both, to set the scale, thus they are not entirely unbiased. Table I summarizes representative model predictions for the masses of the cascade pentaquark that range from 1.75 to 2.07 GeV.

This experiment was mounted at Jefferson Lab to search for the first time for the Φ^{--} exotic pentaquark state in real photoproduction off a neutron target with the subsequent decay into a final state containing three pions and one proton. Early experimental reports on the Θ^+ suggested that photon beams were a rich source of pentaquarks, and one calculation predicted that the production of the Φ^{--} off the neutron was an order of magnitude larger than off the proton [27, 28]. Liu and

* Deceased

† Current address: Argonne National Laboratory, Argonne, Illinois 60441

‡ Current address: Los Alamos National Laborotory, New Mexico, NM

§ Current address: Skobeltsyn Nuclear Physics Institute, Skobeltsyn Nuclear Physics Institute, 119899 Moscow, Russia

¶ Current address: INFN, Sezione di Genova, 16146 Genova, Italy

collaborators computed the photoproduction cross section $\sigma(\gamma n \to K^+ K^+ \Phi^{--})$ and $\sigma(\gamma p \to K^0 K^0 \Phi^+)$, which correspond to similar reaction channels for the neutron and proton. At $E_\gamma = 5$ GeV the estimated cross section $\sigma(\gamma n \to K^+ K^+ \Phi^{--})$, assuming positive parity for the exotic states, is between 0.4 and 1.5 nb, depending on the value of the $g_{K^* N \Xi}$ coupling [27]. There exists a large range of predictions for the decay widths and branching ratios of these exotic states [21, 29, 30], but the dominant decay mode is expected to lead to the ground state cascade $\Phi^{--} \to \pi^- \Xi^-$. In addition, the bias is that the states are very narrow and therefore long-lived, which is particularly interesting, because they are above the free particle decay thresholds. Therefore, our search was targeted to identify states with intrinsic widths that are smaller than the experimental resolution.

II. EXPERIMENT

The purpose of this experiment is to search specifically for the $\Phi^{--}(1860)$ state of the spin-$\frac{1}{2}$ anti-decuplet with the CLAS detector [31] in Hall B at Jefferson Lab in a photoproduction experiment. The acceptance and resolution of CLAS is better for charged than for neutral particles. The most promising topology for our experiment results from the decay sequence

$$\Phi^{--} \to \pi^- \Xi^- \to \pi^-(\pi^- \Lambda) \to \pi^- \pi^-(\pi^- p) . \quad (1)$$

The bremsstrahlung photon beam produced by a 5.77 GeV electron beam interacts with the deuteron target, producing a large variety of final states. The outgoing particles are detected and reconstructed in the CLAS detector. The energy and the interaction time of the initial photon is determined by registering the electron in the Hall B photon tagging facility [32].

The analysis strategy is to directly reconstruct the decay sequence (1) from the final state particles detected in CLAS. First, we identify the $\Lambda(1116)$ using the proton and a π^-. Then we search for the $\Xi^-(1321)$ by combining the $\Lambda(1116)$ with another negative pion. Finally, we analyze the invariant mass of the $\Xi^-(1321)\pi^-$ composite system to search for the Φ^{--} pentaquark state.

This CLAS experiment collected data during 40 calendar days at the end of 2004 and the beginning of 2005, amounting to approximately 25 pb^{-1} integrated luminosity in the tagged photon energy range 4.5 GeV $\leq E_\gamma \leq$ 5.5 GeV. In order to achieve an adequate experimental sensitivity in a reasonable amount of time, we operated at an instantaneous photon flux significantly larger than ever used before with CLAS. The experimental data was carefully analyzed and cross-checked against known cross sections to properly take rate effects into account.
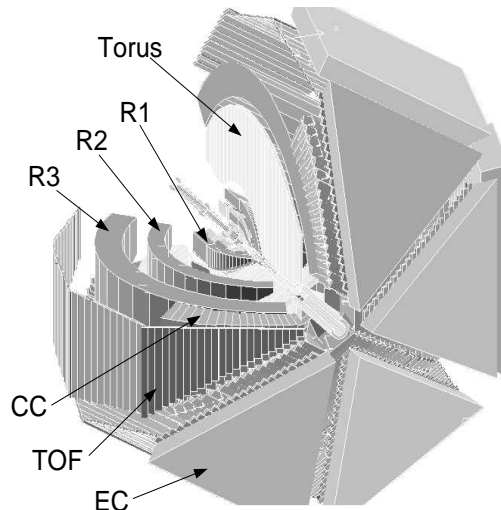

FIG. 1: Three dimensional view of CLAS showing the three regions of Drift Chambers (R1 -R3), Cherenkov Counters(CC), the Time-Of-Flight system (TOF) and the Electromagnetic calorimeter (EC) (see text for details). On this picture, the photon beam travels from the upper-left corner to the lower-right corner.

III. APPARATUS

Hall B at Jefferson Lab houses a photon-tagging system [32] to conduct experiments with real photons. This facility allows for absolute cross section measurements over a broad energy range of the incoming photons. The bremsstrahlung photon beam is produced by the electromagnetic radiation of the primary electron beam in a thin (5×10^{-4} r.l.) radiator. For this experiment, we used the tagged bremsstrahlung beam in Hall B incident on a 40 cm long and 4 cm diameter liquid-deuterium target, which was located on the beam axis 50 cm upstream of the center of the CLAS detector.

CLAS (see Fig. 1) is a nearly 4π detector that is well-suited to study reactions into final states with multiple charged particles. The magnetic field of CLAS [31] is provided by six superconducting coils, which produce an approximately toroidal field in the azimuthal direction around the beam axis. The regions between the cryostats are instrumented with six identical detector packages, also referred to as "sectors". Each sector consists of four Start Counter (ST) paddles [33] mainly used for triggering purposes, three regions of Drift Chambers (R1, R2, and R3) [34] to determine the trajectories of the charged particles, Čerenkov Counters (CC) [35] for electron identification, Scintillator Counters (SC) [36] for charged particle identification based on the Time-Of-Flight (TOF) method, and Electromagnetic Calorimeters (EC) [37] used for electron identification and detection of neutral particles.

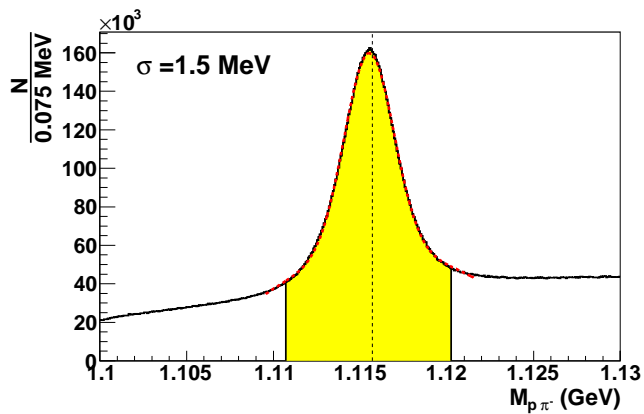The CLAS detector provides a typical momentum res-

FIG. 2: (Color online) Mass spectrum of the $p\pi^-$ system. The yellow shaded area indicates the mass range used in this analysis. The red curve is the fit to a Gaussian peak with a polynomial background. The dashed vertical line shows the PDG [4] value for the mass of $\Lambda(1116)$.

FIG. 3: (Color online) β versus momentum of the negative hadrons. The pions from decays of the Λ candidates are not included in this plot. The magenta lines indicate the π^- identification cuts applied in this analysis.

olution of about 0.6% depending on the kinematics [31] and up to 80% of 4π solid-angle coverage. The efficiency for detection and reconstruction of charged particles in fiducial regions of CLAS is greater than 95%. The combined information from the tracking in Drift Chambers and Scintillator Counters allows us to reliably separate protons from positive pions for momenta up to 3 GeV.

IV. ANALYSIS

A. Event selection

One of the main goals of the analysis procedure is to select events corresponding to the reaction

$$\gamma d \rightarrow \Phi^{--} X, \qquad (2)$$

where we consider the decay sequence (1), and kaons in the final state are not required to be reconstructed.

The $\Lambda(1116)$ candidates are identified by considering every pair of positive and negative tracks with a hypothesis that these are the proton and the negative pion from a $\Lambda(1116)$ decay using timing information from the scintillation counters and momentum and vertex information from tracking. To select the Λ-hyperon, an invariant mass cut 1.1108 GeV $< M_{p\pi^-} <$ 1.1202 GeV is applied as shown in Fig. 2. Because the decay products originate from the same point in space, a 5 cm cut is applied on the Distance-Of-Closest-Approach (DOCA) for the two tracks. We define DOCA as the length of the shortest line segment connecting the trajectories of these two tracks in the vicinity of the CLAS target. The detector resolution for the DOCA between the proton and the π^- is about 1.5 cm. This cut reduces the contributions from $p\pi^-$ pairs that do not come from the $\Lambda(1116)$ decay. If there is more than one $\Lambda(1116)$ candidate, we choose the
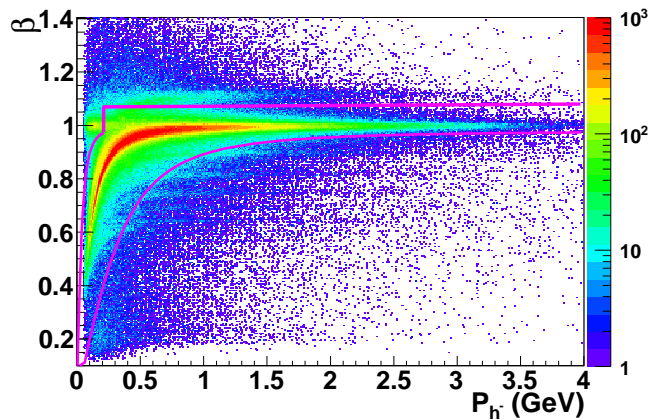
best pair based on the combined information from the matching of the invariant mass and the DOCA between the two tracks.

After selecting the best candidate pair for the $\Lambda(1116)$, we proceed with combining it with the remaining negative pions in the event, which are identified using time-of-flight and tracking information, the event start time determined from the vertex time of the already reconstructed $\Lambda(1116)$, and the reference RF-time from the accelerator's injector. Figure 3 illustrates the negative pion identification used in this analysis. The main band corresponds to the negative pions. The magenta lines show the cuts applied to select the remaining π^-'s in the event. For further analysis, we require that an event contains at least two more negative pions in addition to the π^- in the $\Lambda(1116)$ pair. Therefore, one can have multiple combinations of $(\Lambda\pi^-)$ pairings, and we considered all combinations of the Λ and each of the remaining pions in the event whose track separation in space (DOCA) was sufficiently small. This treatment of the $\Lambda\pi^-$ pairs may lead to multiple entries in the background, but counts the correct pairing in the cascade peak only once.

We also require that the time reconstructed from the event in CLAS matches the time of the interaction determined by the information from the photon tagger. If there is at least one photon detected in the tagger that can provide enough energy for the $d(\gamma, \Xi^-\pi^-)K^+K^+p$ reaction for the measured kinematics, and it is registered within ± 3.2 ns of the interaction time from CLAS, then this event is kept in the data sample. Table II summarizes the event selection cuts used in this analysis.

Figure 4 shows the invariant mass spectrum of the $\Lambda\pi^-$ pairs after the cuts from Table II, with the exception of the cascade mass cut and the DOCA cut in the last two rows. The red dashed and blue dotted lines show the positions of the nominal mass for the $\Xi^-(1321)$ and $\Sigma^-(1385)$, respectively [4]. We apply the

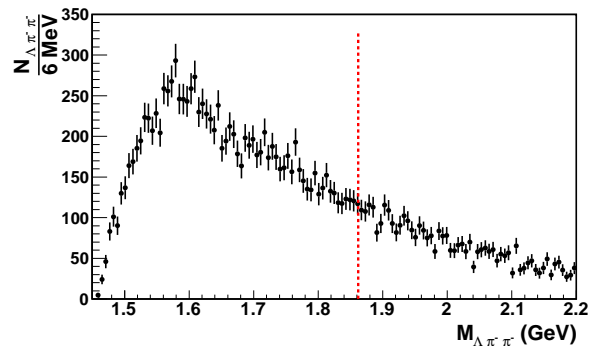|	
DOCA(Λ)	DOCA(Λ) ≤ 5.0 cm
Mass(Λ)	1.1108 GeV $\leq M_\Lambda \leq 1.1202$ GeV
DOCA(Ξ)	DOCA(Ξ) ≤ 4.5 cm
β vs p	p-dependent cut shown in Fig. 3
Tagger time	-3.2 ns $\leq T_\gamma - T_{vtx} \leq +3.2$ ns
Missing Mass	$MM_{\Xi^-\pi^-} > 2M_K + M_p$
Mass(Ξ)	1.3175 GeV $\leq M_{\Lambda\pi^-} \leq 1.3265$ GeV
DOCA($\Xi\pi$)	DOCA($\Xi\pi$) ≤ 4.5 cm

TABLE II: Summary of the event selection.
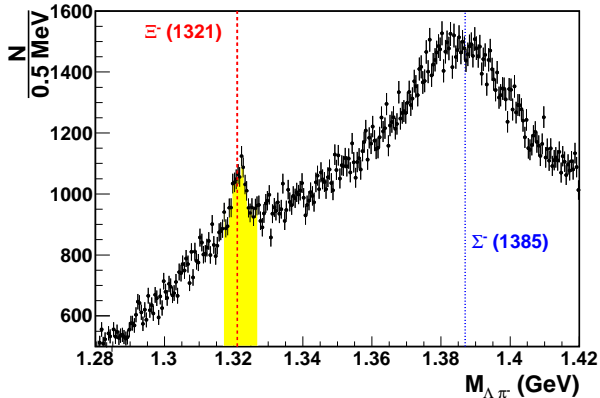
FIG. 4: (Color online) Invariant mass of $\Lambda\pi^-$ pairs. The red dashed and blue dotted lines mark the positions of the nominal mass for $\Xi^-(1321)$ and $\Sigma^-(1385)$, respectively [4]. The shaded area shows the mass range used in this analysis.

FIG. 5: (Color online) Invariant mass of $\Lambda\pi^-\pi^-$ after applying the cascade mass cut. The dashed line marks the position of the reported mass of $\Phi^{--}(1860)$.
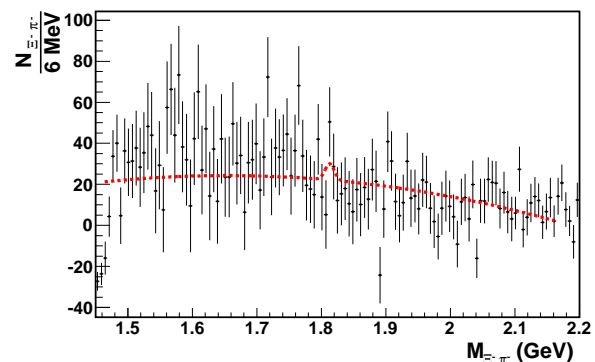
FIG. 6: (Color online) Number of $\Xi^-\pi^-$ events per 6 MeV mass bin. The error bars indicate the statistical uncertainties. The dashed curve shows the fit to a Gaussian peak above a polynomial background. The center of the Gaussian in this plot is fixed at the center of the bin at 1.813 GeV.

1.3175 GeV $\leq M_{\Lambda\pi^-} \leq$ 1.3265 GeV cut illustrated by the shaded area to select events with cascade hyperons. Figure 5 shows the invariant mass of $\Lambda\pi^-\pi^-$ after the cascade mass cut and the cut on the DOCA between the Ξ^- candidate and the negative pion described in Table II. There is no statistically significant structure near the reported mass of the $\Phi^{--}(1860)$. We use the sideband subtraction method to account for the background contribution in the $\Lambda\pi^-\pi^-$ mass spectrum coming from events under the cascade peak in Fig. 4. The $\Lambda\pi^-\pi^-$ spectra from the mass ranges 1.300 GeV $\leq M_{\Lambda\pi^-} \leq$ 1.310 GeV and 1.335 GeV $\leq M_{\Lambda\pi^-} \leq$ 1.345 GeV normalized to the number of background events under the cascade peak are subtracted from the mass spectrum in Fig. 5 to obtain the sideband-subtracted $\Xi^-\pi^-$ mass distribution shown in Fig. 6.

B. Detector simulation

In order to relate the experimental yields to cross sections, acceptance correction factors were calculated using the Monte-Carlo method. The GEANT-based detector simulation package incorporates the survey geometry of CLAS, realistic response of drift chamber and scintillation counters, as well as documented inefficiencies due to dead wires and malfunctioning photomultiplier tubes. Because CLAS is a complex detector covering almost a 4π solid angle, it is virtually impossible to separate the efficiency calculations from the geometrical acceptance calculations. In this paper, the term acceptance correction refers to a combined correction factor due to the geometry of the detector and the inefficiencies of the detection and reconstruction. It is defined as the ratio of the number of reconstructed Monte-Carlo events to the number of simulated events in each given kinematic bin.

The event sample used in the acceptance calculation was generated using a phase-space generator with an event configuration in the first row in Table III without any physics background. Figure 7 shows the invariant mass of the $\Lambda\pi^-$ system from the data (a) and from the simulations (b). The simulated event sample does not contain any background because we are interested only in determining the acceptance and efficiency for the
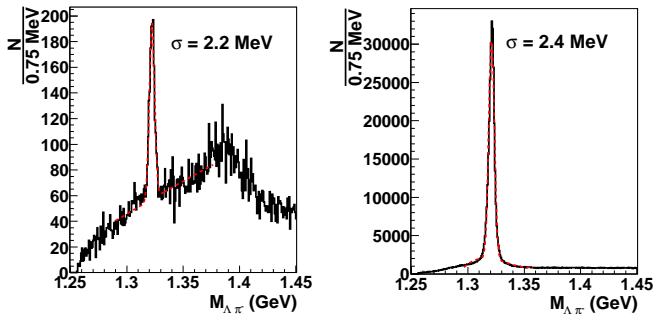
FIG. 7: (Color online) Mass spectrum of $\Lambda\pi^-$ from data (a) using restrictive cuts (see text for details), and $\Lambda\pi^-$ mass from the GEANT-based simulations (b).

FIG. 8: (Color online) Acceptance of CLAS versus the invariant mass of the $\Xi^-\pi^-$ system, determined from the $\gamma d \to K^+K^+\Xi^-\pi^-p_s$ phase space simulation, using a GEANT-based detector simulation package GSIM. The vertical red line indicates the position of the peak seen by the NA49 collaboration.

Row #	Production Model	Relative Acceptance
1	$\gamma d \to K^+K^+\Xi^-\pi^-p_s$	1.00
2	$\gamma d \to K^+\Sigma^-(2650)p_s$ $\to K^+K^+\Phi^{--}p_s \to K^+K^+\Xi^-\pi^-p_s$	+1.24
3	$\gamma d \to K_f^+\Sigma^-(2650)p_s$ $\to K_f^+K^+\Phi^{--}p_s \to K_f^+K^+\Xi^-\pi^-p_s$	+1.47
4	$\gamma d \to K^+K^+\Phi^{--}p_s \to K^+K^+\Xi^-\pi^-p_s$	+1.07

TABLE III: Event configurations used in the Monte-Carlo generator for the model dependence studies. The elementary production is assumed to be from a neutron in a deuterium target and the proton, p_s, is treated as a spectator in the reaction.

events which contain cascade hyperons. The acceptance and efficiency corrections calculated for events containing $\Xi^-\pi^-$ are applied to the sideband-subtracted spectrum. Event selection criteria for the plots in Fig. 7 are stricter than the nominal cuts in this analysis to enhance the signal-to-background ratio for the ground state cascade peak for a visual comparison of the data with the simulations.

C. Model dependence

Because we do not know how the cross section of the $\Phi^{--}(1860)$ photoproduction depends on kinematics, and since we integrate over all of the kinematic variables, our estimate of the CLAS acceptance depends on the choice of the distribution of the events over the accessible phase space. In order to estimate the uncertainty of the acceptance due to the model dependence, we studied four event configurations; the relative acceptances are given in Table III. The events were generated using a software package that includes essentially no specific dynamics and mainly simulates events according to phase-space probabilities. The reaction in row 1 of Ta-
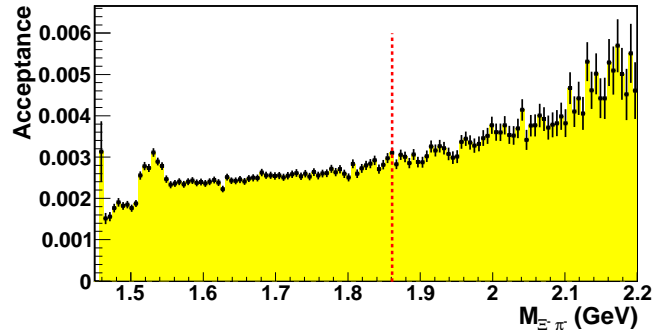
ble III is a four-body phase-space uniform distribution complemented with a spectator proton with Fermi momentum smearing according to Ref. [38]. For the process in row 2, a hypothetical $\Sigma^-(2650)$ was implemented in the event generator, which decays into $K^+\Phi^{--}(1860)$ with a total width of 35 MeV. The $\Phi^{--}(1860)$ is simulated as a particle with an infinitely narrow width at mass $M_\Phi = 1.862$ GeV that decays only through the $\Xi^-\pi^-$ channel. The reactions in rows 2 and 4 are simulated according to two- and three-body phase space, respectively, with a Fermi-smeared spectator proton momentum spectrum according to Ref. [38]. The process in row 3 of Table III is simulated according to two-body phase-space but with an additional exponential t-dependence for the K^+ with a t-slope parameter $b = 2.6$ GeV^{-2}. The flat phase space provides an estimate of the acceptance for s-channel processes, while including a steeper t-dependence allows us to consider the processes going through the t-channel exchanges. For the processes in rows 2 to 4, the acceptance is estimated at a fixed mass $M_{\Xi^-\pi^-} = 1.862$ GeV, since the process explicitly includes the $\Phi^{--}(1860)$ decay. Using this table, we calculate the root-mean-square (RMS) of the differences in the acceptance at $M_{\Xi^-\pi^-} = 1.862$ GeV, and we assign a relative uncertainty of $\frac{\sigma_A^{sys}}{A}$ of 21% due to model dependence. This is the largest source of uncertainty in the determination of the cross sections and its upper limits.

The acceptance of CLAS versus the invariant mass of the $\Xi^-\pi^-$ system calculated using the process in row 1 of Table III is shown in Fig. 8. At the expected Φ^{--} mass $M = 1.862$ GeV, the acceptance does not exhibit any special features and is about 0.3%. The artificial enhancement near mass $M = 1.53$ GeV is due to pion combinatorics and the mass cut to select $\Xi^-(1321)$ events.

D. Trigger conditions and normalization

The process of interest for this experiment is $\gamma d \to p\pi^-\pi^-\pi^- X$, where three charged pions and a proton are detected in CLAS. To be able to run at higher photon-deuteron luminosities, we used a highly selective trigger, so that the data acquisition system could cope with the data rate. After extensive studies, we decided to require at least three charged particles in three different sectors of CLAS to be detected in the Start Counter and TOF system in the main trigger. But we also took data with a two-sector trigger to quantify trigger inefficiencies, which was prescaled by a factor of 5 to 20, depending on the running conditions. The trigger required a time coincidence of tracks in CLAS with a signal from the photon tagger, signaling the production of a photon in the energy range of 4.5 to 5.5 GeV.

The primary trigger condition suffered from inefficiencies at high luminosity. These inefficiencies were determined empirically by studying the luminosity dependence of Λ production and also by comparing these yields with those measured with the two-sector trigger, corrected for the prescale factor. The study used events containing an identified Λ-hyperon, decaying to a proton and a pion, and two additional reconstructed tracks, similar to our sample of signal events. The average inefficiency of the three-track trigger varied linearly with the electron beam current up to 35%, with an average of 25% at the nominal current of 30 nA. The yields normalized by this factor correspond to those obtained from the two-track trigger, which did not exhibit any dependence on luminosity.

The overall normalization of the experiment was checked using the $d(\gamma, \pi^- \Delta^{++})n$ reaction with the detection of the $\pi^+\pi^- p$ final state. The cross section of this process is expected to be mostly dominated by photoproduction off a quasi-free proton $\gamma p \to \pi^- \Delta^{++}$. Although final state interactions (FSI) contribute to this process, we do not expect their impact to be significant within the precision required for this purpose. Using the same analysis and assumptions, the measured cross sections for $d(\gamma, \pi^- \Delta^{++})n$ obtained from the current data was compared to the $p(\gamma, \pi^- \Delta^{++})$ cross section from a different CLAS run period where these trigger inefficiencies were not present. The cross sections from the two CLAS data sets for the photon energy range of 4.5 GeV $< E_\gamma <$ 5.0 GeV differed by $9-14\%$. The agreement of our measurements with the published data on $\gamma p \to \pi^- \Delta^{++}$ from SAPHIR at E_γ=2.5 GeV [39] is better than 10%, which indeed indicates that FSI contributions are negligible. A more detailed analysis of the $d(\gamma, \pi^+\pi^- p)n$ reaction and its cross section is under way [40]. Based on these comparisons, we have assigned the normalization uncertainty of $\pm15\%$ for the presented data.

Source of Uncertainty	Uncertainty (σ)
Model dependence of acceptance	21%
Flux and trigger efficiency	15%
Total in quadrature	26%

TABLE IV: Dominant sources and the values of the relative systematic uncertainties. The overall systematic uncertainty calculated as the square root of the quadrature sum is $\pm26\%$.

E. Systematic uncertainties

The final invariant mass spectrum of $\Xi^-\pi^-$ was studied for various values of the selection parameters for the Λ, Ξ, and π^-. These variations did not result in any qualitative change of the invariant mass distributions of $\Lambda\pi^-\pi^-$ or $\Xi^-\pi^-$. We checked the sensitivity of the results with respect to the following parameters: selection parameters for the Λ-candidates, cuts on time matching between the event in CLAS and hit in the tagger counter, DOCA cuts on the Λ and the Ξ^- candidates, detached vertex cuts for the reconstructed Λ, and particle identification cuts on β versus p. The choice of these analysis parameters did not affect the final result for the upper limit of the cross sections, and we therefore considered their uncertainties to be negligible.

The uncertainty in the overall normalization of the experiment is driven by the relatively large trigger efficiency corrections that are required, as described previously. We assign an uncertainty of $\pm15\%$ to the absolute normalization, which is estimated by comparing our determination of Δ^{++} production to other measurements, as discussed in the previous section.

The dominant contribution to the photoproduction cross section systematic uncertainty comes from the model dependence of the estimated acceptance, and we take the RMS of the model calculations to obtain a $\pm21\%$ relative uncertainty.

Table IV summarizes the dominant contributions to the systematic uncertainties. We used the sum in quadrature of 26% to determine the upper limits for the experimental cross sections described in the next section.

V. UPPER LIMITS

In order to determine the upper limits for the cross section for a possible peak, we scanned each 6 MeV-wide bin in the sideband-subtracted mass spectrum in Fig. 6, considering the center of each bin as the mean value of a Gaussian distribution with a fixed width of $\sigma_G = 7$ MeV, which represents our experimental resolution for a potential $\Phi^{--}(1860)$, as estimated by the detector simulation. Then the points in the neighborhood of the bin are fitted to a Gaussian peak plus a second-order polynomial. The purpose of this χ^2-fit is to provide us with an estimate of the background under the possible peak and its un-
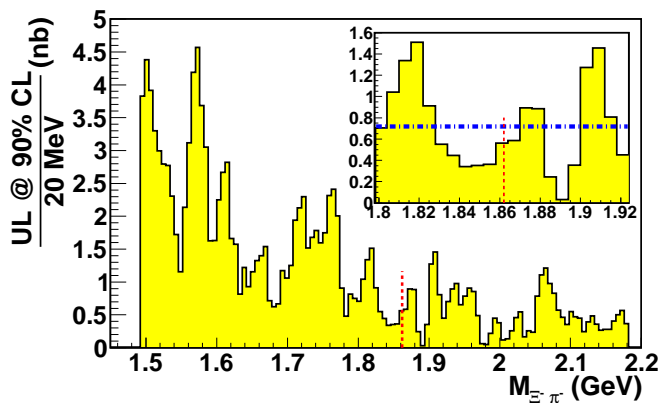
FIG. 9: (Color online) Upper limits for the photoproduction cross section with subsequent decay $\Phi^{--} \to \Xi^- \pi^-$ in 20 MeV mass windows at 90% CL versus the invariant mass of $\Xi^- \pi^-$. The red dashed vertical line marks the position of the enhancement reported by NA49 .

certainty. The background level is taken from the fitted polynomial excluding the Gaussian. The total number of signal events is calculated as the excess of the observed events over the fitted background, both integrated within a window of 20 MeV around the center of each bin. The red dashed curve in Fig. 6 shows a particular example of the fit for a mass bin centered at $M_{\Xi^- \pi^-} = 1.813$ GeV.

In order to obtain an upper limit on the photoproduction cross section, we developed a procedure based on the method described in Ref. [41]. This procedure allows us to factor in the uncertainties in the background extraction and the acceptance correction into the determination of the upper limits at a given confidence level (CL) using the sideband-subtracted method. We also performed a cross check of our method with an approach for estimating the upper limits by Smith [42] based on the construction prescription of the Feldman-Cousins method [43], which properly takes into account the systematic uncertainties when constructing the confidence belts. For a comparison, we assumed a mass-independent acceptance of 0.4% and a mass-independent relative acceptance uncertainty of 30%; the agreement between the two methods is very good. A more detailed description of our method to determine the upper limits can be found in Appendix A.

The upper limit of the photoproduction cross section

at 90% confidence level for the process $\gamma d \to \Phi^{--} X \to \Xi^- \pi^- X$ versus invariant mass of the $\Xi^- \pi^-$ system is shown in Fig. 9. In the mass range near $M = 1.862$ GeV, where the NA49 collaboration observed an enhancement, we obtain a 90% CL upper limit of 0.7 nb.

VI. SUMMARY

In conclusion, we have conducted for the first time a search for the $\Phi(1860)^{--}$ pentaquark state in real photoproduction within the incident photon energy range 4.5 GeV $\leq E_\gamma \leq$ 5.5 GeV. We do not observe any statistically significant enhancement near invariant mass $M = 1.862$ GeV. The upper limit at 90% confidence for the photoproduction cross section of the reaction $\gamma d \to \Phi^{--} X$ multiplied by the branching ratio for $\Phi^{--} \to \Xi^- \pi^-$ is determined as a function of the invariant mass of $\Xi^- \pi^-$, using a method similar to the one described in Ref. [41]. The upper limit for the cross sections for Φ^{--} photoproduction with subsequent decay $\Phi^{--} \to \Xi^- \pi^-$ for 20 MeV mass windows is less than 3 nb in the $\Xi^- \pi^-$ mass range between 1.6 GeV and 1.9 GeV. The upper limit is less than 1.5 nb for the masses from 1.9 GeV to 2.2 GeV. The upper limit for the cross section averaged within a narrow mass range of 1.80 GeV $< M_{\Xi\pi} < 1.92$ GeV is 0.7 nb. This is approximately a factor of three improvement over the previously estimated upper limit in small-angle electroproduction by the HERMES collaboration of about 2 nb [7].

[1] T. Nakano *et al.*, Phys. Rev. Lett. **91**, 012002 (2003).
[2] D. Diakonov, V. Petrov, and M. Polyakov, Z. Phys. A **359**, 305 (1997), [hep-ph/9703373].
[3] K. H. Hicks, Prog. Part. Nucl. Phys. **55**, 647 (2005).
[4] K. Nakamura *et al.*, J. Phys. **G37**, 075021 (2010).
[5] C. Alt *et al.*, Phys.Rev.Lett. **92**, 042003 (2004).
[6] M. Adamovich *et al.*, Phys.Rev. **C70**, 022201 (2004).

[7] A. Airapetian *et al.*, Phys.Rev. **D71**, 032004 (2005).
[8] S. Chekanov *et al.*, Phys.Lett. **B610**, 212 (2005).
[9] E. Ageev *et al.*, Eur.Phys.J. **C41**, 469 (2005).
[10] K. Knopfle, M. Zavertyaev, and T. Zivko, J.Phys.G **G30**, S1363 (2004).
[11] B. Aubert *et al.*, Phys.Rev.Lett. **95**, 042002 (2005).
[12] K. Stenson, Int.J.Mod.Phys. **A20**, 3745 (2005).

[13] J. Link *et al.*, Phys.Lett. **B661**, 14 (2008).
[14] A. Abulencia *et al.*, Phys.Rev. **D75**, 032003 (2007).
[15] S. Schael *et al.*, Phys.Lett. **B599**, 1 (2004).
[16] P. Achard *et al.*, Eur.Phys.J. **C49**, 395 (2007).
[17] A. Aktas *et al.*, Eur.Phys.J. **C52**, 507 (2007).
[18] J. Abdallah *et al.*, Phys.Lett. **B653**, 151 (2007).
[19] A. Aleev *et al.*, Phys.Atom.Nucl. **70**, 1527 (2007).
[20] D. Christian *et al.*, Phys.Rev.Lett. **95**, 152001 (2005).
[21] D. Diakonov and V. Petrov, Phys. Rev. **D69**, 094011 (2004).
[22] R. L. Jaffe and F. Wilczek, Phys. Rev. Lett. **91**, 232003 (2003).
[23] M. Karliner and H. J. Lipkin, Phys. Lett. **B575**, 249 (2003).
[24] J. R. Ellis, M. Karliner, and M. Praszalowicz, JHEP **05**, 002 (2004).
[25] R. Jaffe and F. Wilczek, Phys. Rev. **D69**, 114017 (2004).
[26] S. K. Majee and A. Raychaudhuri, Phys. Rev. **D77**, 074016 (2008).
[27] W. Liu and C. Ko, Phys. Rev. C **69**, 045204 (2004), [nucl-th/0312119].
[28] C. M. Ko and W. Liu, (2004), nucl-th/0410068.
[29] C. E. Carlson, C. D. Carone, H. J. Kwee, and V. Nazaryan, Phys. Lett. **B579**, 52 (2004).
[30] Y.-S. Oh, H. C. Kim, and S. H. Lee, Phys. Rev. **D69**, 094009 (2004).
[31] B. A. Mecking *et al.*, Nucl. Instrum. Meth. **A503**, 513 (2003).
[32] D. I. Sober *et al.*, Nucl. Instrum. Meth. **A440**, 263 (2000).
[33] Y. G. Sharabian *et al.*, Nucl. Instrum. Meth. **A556**, 246 (2006).
[34] M. D. Mestayer *et al.*, Nucl. Instrum. Meth. **A449**, 81 (2000).
[35] G. Adams *et al.*, Nucl. Instrum. Meth. **A465**, 414 (2001).
[36] E. S. Smith *et al.*, Nucl. Instrum. Meth. **A432**, 265 (1999).
[37] M. Amarian *et al.*, Nucl. Instrum. Meth. **A460**, 239 (2001).
[38] W. R. Gibbs, Phys. Rev. **C70**, 045208 (2004).
[39] C. Wu *et al.*, Eur. Phys. J. **A23**, 317 (2005).
[40] L. Graham, in preparation (unpublished).
[41] W. A. Rolke, A. M. Lopez, and J. Conrad, Nucl. Instrum. Meth. **A551**, 493 (2005).
[42] E. S. Smith, Nucl. Instrum. Meth. **A604**, 729 (2009).
[43] G. J. Feldman and R. D. Cousins, Phys. Rev. **D57**, 3873 (1998).

Appendix A: Appendix: Determination of upper limits

The number of events in the 20 MeV mass windows from the sideband-subtracted spectrum in Fig. 6 are distributed according to a Gaussian distribution with a width determined by the statistical uncertainty obtained during the sideband subtraction. Therefore, in each mass window we model the excess of the events above the background, or signal events, according to a Gaussian distribution, with a mean $\mu \geq 0$ limited by the condition that the cross section cannot be negative even if the number of observed events is less than the expected background.

Systematic uncertainties are included into the calculation by assuming that the measured acceptance and the number of background events are random variables distributed according to the normal distribution:

$$
\begin{aligned}
P(x, b_m, e_m \mid \mu, b, e) \; = \; & \frac{1}{\sqrt{2\pi}\sigma_x} e^{-\frac{(e\mu + b - x)^2}{2\sigma_x^2}} \quad \text{(A1)} \\
& \times \; \frac{1}{\sqrt{2\pi}\sigma_b} e^{-\frac{(b_m - b)^2}{2\sigma_b^2}} \\
& \times \; \frac{1}{\sqrt{2\pi}\sigma_e} e^{-\frac{(e_m - e)^2}{2\sigma_e^2}} \; ,
\end{aligned}
$$

where μ is the expectation of the number of signal events, e is the acceptance factor for the signal, b is the expectation value of the number of background events in the 20 MeV mass window, and x is the observed number of events in the same window for each fit. The experimental statistical uncertainty is denoted by σ_x. The estimated number of background events b_m is determined from the polynomial fits to the background, as shown in Fig. 6, and its uncertainty, σ_b, is taken from errors returned from the fit. The estimated signal acceptance e_m is determined by Monte Carlo and shown in Fig. 8. For the uncertainty in the value of e_m, σ_e, we use the systematic uncertainty of 26% (Table IV). $P(x, b_m, e_m \mid \mu, b, e)$ is the probability, under assumption of our model, to observe the values x, b_m and e_m. Similar to the Rolke method in Ref. [41] we use a profile likelihood to estimate the confidence level (CL). The logarithm of the profile likelihood is defined as the logarithm of the ratio

$$
\begin{aligned}
\mathcal{L} \; = \; & -2\ln\lambda(\mu_t) \\
= \; & -2\ln\left(\frac{\sup\{P(x, b_m, e_m \mid \mu_t, b, e); b, e\}}{\sup\{P(x, b_m, e_m \mid \mu, b, e); \mu, b, e\}} \right) \\
= \; & \frac{(\mu_t e_m + b_m - x)^2}{\sigma_x^2 + \mu_t^2 \sigma_e^2 + \sigma_b^2} \; , \quad \text{(A2)}
\end{aligned}
$$

where λ is the profile likelihood, and μ_t is the hypothesis value being tested. The supremum, or the least upper bound, $\sup\{P(x, b_m, e_m \mid \mu_t, b, e); \mu, b, e\}$ in the denominator under the logarithm in Eq. A2 is taken over all values of (μ, b, e), and is located at $\left(b = b_m, e = e_m, \mu = \frac{x - b}{e} \right)$. The least upper bound $\sup\{P(x, b_m, e_m \mid \mu, b, e); b, e\}$ in the numerator is taken only over the background and efficiency b and e. In order to determine the location of this supremum we find the zero-crossings of both partial derivatives of the likelihood P in Eq. A2: $\frac{\partial P}{\partial b} = 0$ and $\frac{\partial P}{\partial e} = 0$. In the limiting case when the background is known to be zero and the efficiency is 100%, Eq. A2 simply becomes

$$
\mathcal{L} \; = \; \frac{(\mu_t - x)^2}{\sigma_x^2} \; . \quad \text{(A3)}
$$

The log-likelihood distribution in Eq. A2 is approximated by the χ^2-distribution ($\chi^2 \approx \mathcal{L}$) with the appropriate number of degrees of freedom. In this case, there is
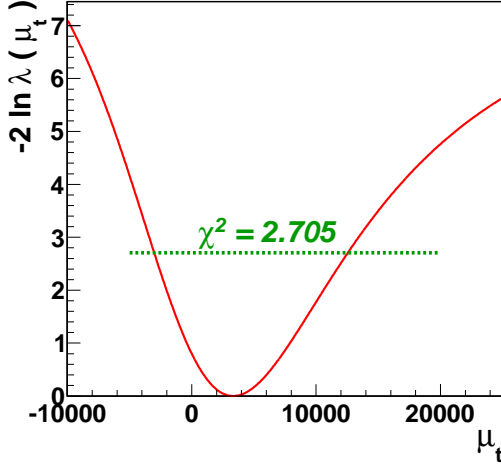
FIG. 10: (Color online) Illustration of determining the upper and lower limits for $CL = 90\%$. The x-axis is the expectation value for the measured quantity μ. The red solid curve is the logarithm of the profile likelihood $\mathcal{L}$ versus μ_t, and the green dashed line is $\chi^2 = 2.705$ corresponding to $CL = 90\%$.

only one degree of freedom. To find the values of μ_t corresponding to a certain confidence level, one first finds the χ^2 value corresponding to that CL for the χ^2-distribution with a single degree of freedom. The solutions for μ_t are the values where $\mathcal{L}$ differs from its minimum by that amount of χ^2. The solution that is less than the most likely value of μ is the lower limit, while the larger solution is the upper limit. After substituting χ^2 for $\mathcal{L}$ in Eq. (A2) and solving the quadratic equation, the two solutions for μ_t for a given χ^2 can be found as follows:

$$
\begin{aligned}
\mu_t \;=\; & \frac{-b_m\, e_m + x e_m}{\chi^2 \sigma_e^2 - e_m^2} + \big(e_m^2\, \chi^2 \sigma_x^2 + e_m^2 \chi^2 \sigma_b^2 \quad \text{(A4)} \\
& - \; 2\chi^2 \sigma_e^2 x b_m + \chi^2 \sigma_e^2 x^2 - \chi^4 \sigma_e^2 \sigma_x^2 + \chi^2 \sigma_e^2 b_m^2 \\
& - \; \chi^4 \sigma_e^2 \sigma_b^2 \big)^{\frac{1}{2}} \times \big(\chi^2 \sigma_e^2 - e_m^2 \big)^{-1} \;.
\end{aligned}
$$

Fig. 10 illustrates how the upper and lower limits at 90% CL are found. The red curve is the log-likelihood $\mathcal{L}$ with a minimum at around $\mu_t \approx 3300$, which is the most likely value for the illustrated example. The probability of having 90% of the trials within a certain range is realized for $\chi^2 = 2.705$, which is represented by the green line in Fig. 10. The intersection points of these curves give us the upper and lower limits at 90% confidence level. In certain cases, for instance when the estimated efficiency is very low, and the uncertainty for it is relatively large, no upper or lower limits can be found. This happens when the logarithm of the profile likelihood $\mathcal{L}$ does not behave like a parabola, and therefore is not well approximated by the χ^2-distribution.

In cases where the most likely μ_t is negative, we take the lower limit to be 0. If the most likely value μ_t and the upper limit are negative, we increment the number of observed events x by one unit until we get the first positive value. Such an ad hoc adjustment can cause the coverage probability, defined as the probability that a true value of the cross section for a process is less than the corresponding upper limit obtained by this method, to differ from the desired confidence level of 90%. Therefore, one needs to check that the results obtained by this procedure indeed provide the desired confidence level. Our Monte-Carlo tests showed that the coverage probability of this method is within 5% of the nominal confidence level.